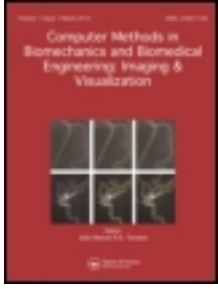


This article was downloaded by: [Czech Academy of Sciences]

On: 02 June 2014, At: 05:12

Publisher: Taylor & Francis

Informa Ltd Registered in England and Wales Registered Number: 1072954 Registered office: Mortimer House, 37-41 Mortimer Street, London W1T 3JH, UK



Computer Methods in Biomechanics and Biomedical Engineering: Imaging & Visualization

Publication details, including instructions for authors and subscription information:

<http://www.tandfonline.com/loi/tciv20>

Model-based extraction of input and organ functions in dynamic scintigraphic imaging

Ondřej Tichý^a, Václav Šmídl^a & Martin Šámal^b

^a Institute of Information Theory and Automation, Adaptive Systems, Pod Vodárenskou věží 4, Prague 182 08, Czech Republic

^b Institute of Nuclear Medicine, Charles University Prague, Salmovská 3, Prague 12000, Czech Republic

Published online: 28 May 2014.

To cite this article: Ondřej Tichý, Václav Šmídl & Martin Šámal (2014): Model-based extraction of input and organ functions in dynamic scintigraphic imaging, *Computer Methods in Biomechanics and Biomedical Engineering: Imaging & Visualization*, DOI: [10.1080/21681163.2014.916229](https://doi.org/10.1080/21681163.2014.916229)

To link to this article: <http://dx.doi.org/10.1080/21681163.2014.916229>

PLEASE SCROLL DOWN FOR ARTICLE

Taylor & Francis makes every effort to ensure the accuracy of all the information (the "Content") contained in the publications on our platform. However, Taylor & Francis, our agents, and our licensors make no representations or warranties whatsoever as to the accuracy, completeness, or suitability for any purpose of the Content. Any opinions and views expressed in this publication are the opinions and views of the authors, and are not the views of or endorsed by Taylor & Francis. The accuracy of the Content should not be relied upon and should be independently verified with primary sources of information. Taylor and Francis shall not be liable for any losses, actions, claims, proceedings, demands, costs, expenses, damages, and other liabilities whatsoever or howsoever caused arising directly or indirectly in connection with, in relation to or arising out of the use of the Content.

This article may be used for research, teaching, and private study purposes. Any substantial or systematic reproduction, redistribution, reselling, loan, sub-licensing, systematic supply, or distribution in any form to anyone is expressly forbidden. Terms & Conditions of access and use can be found at <http://www.tandfonline.com/page/terms-and-conditions>

Model-based extraction of input and organ functions in dynamic scintigraphic imaging

Ondřej Tichý^{a*}, Václav Šmídl^{a1} and Martin Šámal^{b2}

^a*Institute of Information Theory and Automation, Adaptive Systems, Pod Vodárenskou věží 4, Prague 182 08, Czech Republic;* ^b*Institute of Nuclear Medicine, Charles University Prague, Salmovská 3, Prague 12000, Czech Republic*

(Received 22 January 2014; accepted 15 April 2014)

Image-based definition of input function (IF) and organ function is a prerequisite for kinetic analysis of dynamic scintigraphy or positron emission tomography. This task is typically done manually by a human operator and suffers from low accuracy and reproducibility. We propose a probabilistic model based on physiological assumption that time–activity curves (TACs) arise as a convolution of an IF and tissue-specific kernels. The model is solved via the Variational Bayes estimation procedure and provides estimates of the IF, tissue-specific TACs and their related spatial distributions (images) as its results. The algorithm was tested with data of dynamic renal scintigraphy. The method was applied to the problem of differential renal function estimation and the IF estimation and the results are compared with competing techniques on datasets with 99 and 19 patients. The MATLAB implementation of the algorithm is available for download.

Keywords: blind source separation; convolution; dynamic medical imaging; compartment modelling

1. Introduction

Quantitative kinetic analysis of medical structures is often based on source separation of dynamic image sequences from various modalities. The sequence of images allows to study changes in the images in time which allows to quantify a kinetic parameter of the studied organs. In this paper, we assume that the organ images have time-invariant shape and we observe only temporal changes in organ activities. This approach is widely used in dynamic scintigraphy (Di Paola et al. 1982) or positron emission tomography (Margadán-Méndez et al. 2010). The analysis is typically performed in two steps. First, time–activity curves (TACs) of the organs or tissues of interest are extracted from the dynamic image sequence, and kinetic analysis is performed on these data. The standard kinetic analysis requires two types of TACs: (i) the input function (IF), reflecting the changes of tracer concentration in the blood and (ii) organ functions, reflecting the changes of tracer concentration in a specific organ or tissue (Patlak et al. 1983; Vriens et al. 2009).

In practice, the IF can be directly measured by sampling the arterial blood (Greuter et al. 2003). This approach needs a medical intervention which is often not appropriate in clinical practice. This invasive procedure can be substituted by extraction of the IF from the observed images. However, the IF is not observed directly, and its extraction from the observed images is not unique. Existing state-of-the-art techniques are based on manual selection of regions of interest (ROIs) in the observed images. The IF can be extracted from a ROI placed directly on the heart, if available, or on other vascular

structures if they can be recognised on the images (Germano et al. 1992). TACs of the organ functions are also usually obtained by user-defined ROIs placed manually on the organs of interest. This approach suffers from subjectivity, low accuracy and poor reproducibility (Caglar et al. 2008; Brink et al. 2012). Despite the operator intuitively tending to avoid image areas with tissue overlaps that represent mixtures of different organ kinetics, it is often impossible to exclude them simply because no regions that would manifest pure IF or specific organ function exist in the analysed image. User-independent decomposition of dynamic image sequences into organ-specific images and associated TACs is thus a prerequisite for more reliable quantitative analysis of both clinical examinations and research experiments.

Automatic, or semi-automatic methods for ROI selection are available (Garcia et al. 2010); however, they are not completely reliable and the activity is always counted from the full area of the ROI which may still include some background organs. An alternative approach is to use blind source separation (BSS) methods. They have no physiological assumption in their basic form, (Miskin 2000); however, some extensions have also been proposed (Chen et al. 2011; Riabkov and Di Bella 2002). The aim of this work is to design a mathematical model that integrates all common assumptions of the domain and to use this model to create a new BSS method for this particular task. The model is designed to include convolution of the IF and tissue-specific kernels. The IF and the kernel parameters are considered to be unknown. They are estimated from the observed images using the

*Corresponding author. Email: otichy@utia.cas.cz

presented BSS method based on the Variational Bayes (VB) approach (Šmídl and Quinn 2006).

The proposed method is tested in three situations. First, it is used to create a semi-automated procedure for estimation of differential renal function (DRF). Suitability of the procedure is studied on a dataset of 99 patients (VFN Praha 2013). For comparison, the same data were analysed using manual ROI placement by an expert and by a trained novice as well as the state-of-the-art algorithms of BSS such as (Miskin 2000) or (Šmídl and Tichý 2012). Second, we compare the estimated TACs from the competing algorithms with those TACs obtained by an experienced physician on a dataset of 19 patients where the manual estimates from a physician are available. Third, estimated IFs from ROIs of left and right kidneys using the proposed method are compared in order to study the consistency of estimates.

2. Methods

The goal of the designed method is to automatically identify tissue structures and their related TACs from the observed sequence of images. The estimation procedure is based on a probabilistic model that is designed using common assumptions used in nuclear medicine. These assumptions are the following: (i) the observed image is a superposition of the underlying tissue images, (ii) the TACs are described by a compartment model, where each TAC arises as a convolution between a common IF and a tissue-specific kernel (Riabkov and Di Bella 2002), (iii) the tissue images and the TACs are non-negative and (iv) the variance of the observation noise is identical for all pixels. Assumption (iv) can be easily relaxed for signals with noise proportional to the signal strength by using the correspondence analysis preprocessing (Benali et al. 1993). These assumptions are now formulated mathematically via a probabilistic model. The VB methodology is used to estimate all unknown parameters of the proposed model.

2.1 Mathematical model assumptions

The observed sequence of images is indexed by a discrete time index t , the number of images in the sequence is n . The sequence is assumed to be composed of r underlying tissues indexed by symbol $f = 1, \dots, r$, r is unknown. Each observed image is stored in one vector \mathbf{d}_t with the pixels stored column-wise and is assumed to be a sum of contributions from the underlying tissues

$$\mathbf{d}_t = \sum_{f=1}^r \mathbf{a}_f x_{t,f}, \quad (1)$$

where \mathbf{a}_f are the tissue image in the same vector form as the observed image, and $x_{t,f}$ is the activity of the f th tissue

at time t . The TAC \mathbf{x}_f , i.e. the organ function, is supposed to be the result of convolution of the common IF, \mathbf{b} , and a tissue-specific kernel, \mathbf{u}_f . The tissue-specific kernels, \mathbf{u}_f , are modelled using increments \mathbf{w}_f as suggested in Kuruc et al. (1982), hence

$$x_{t,f} = \sum_{i=1}^t b_{t-i+1} u_{i,f}, \quad u_{t,f} = \sum_{i=t}^n w_{i,f}, \quad (2)$$

and

$$w_{i,f} = \begin{cases} h_f & s_f \leq t \leq s_f + l_f \\ 0 & \text{otherwise,} \end{cases}$$

where \mathbf{w}_f is the f th tissue-specific vector with non-negative elements with specified structure. Here, h_f is the height of each increment in the f th tissue, s_f is the starting point of the increments and $s_f + l_f$ is the ending point of the increments. In other words, vector \mathbf{w}_f is supposed to be in the form of $[0, \dots, 0, h_f, \dots, h_f, 0, \dots, 0] \equiv M_{\mathbf{w}_f}$.

Following Kuruc et al. (1982), we model the IF \mathbf{b} as a sum of increments:

$$b_t = \sum_{i=t}^n g_i, \quad (3)$$

where \mathbf{g} is vector with increments of the same size as vector \mathbf{b} . The original motivation of Kuruc et al. (1982) was to allow only positive increments \mathbf{g}_i ; however, this assumption is not present in our model.

2.2 Probabilistic model

The deterministic model assumptions in Section 2.1 are valid only approximately. For example, the measurements of \mathbf{d}_t (1) are subject to noise with unknown variance ω . The observed images \mathbf{d}_t are thus random realisations from the probability density:

$$f(\mathbf{d}_t | \omega) = tN \left(\sum_{f=1}^r \mathbf{a}_f x_{t,f}, \omega^{-1} I_p \right), \quad (4)$$

$$f(\omega) = G(\vartheta_0, \rho_0), \quad (5)$$

where p denotes the number of pixels in the image, I_n is the identity matrix of size n , $tN(\cdot, \cdot)$ is the multivariate normal distribution truncated to positive values with a given mean vector and covariance matrix. Following the Bayesian approach, each unknown parameter needs to have a prior distribution of its potential values. The prior distribution of the unknown variance of the observation noise, ω , is assumed to be of the gamma form, $G(\cdot, \cdot)$, with prior parameters ϑ_0, ρ_0 . The choice of distributions from exponential family also known as conjugate priors,

Ghahramani and Beal 2001), is motivated by tractability in VB inference (Šmídl and Quinn 2006).

The convolution kernel (2) may also differ from the assumed form, where variances of the differences \mathbf{w}_f are unknown, denoted ξ_f . The model of the TACs is composed from kernels \mathbf{w}_f and the IF \mathbf{b} . The prior distribution of the f th TAC model is then

$$f(\mathbf{w}_f | \xi_f) = tN(M_{\mathbf{w}_f}, \xi_f I_n), \quad (6)$$

$$f(\xi_f) = G(\kappa_{f,0}, \nu_{f,0}), \quad (7)$$

and $f(h_f) = tN(\mathbf{0}_{r \times 1}, \tau_0)$, $f(l_f | s_f) = U(0, n - s_f)$ and $f(s_f) = U(0, n)$, where the parameters indexed with zero are assumed to be known prior parameters, $\mathbf{0}_{n \times 1}$ denotes zero matrix of the respected size and $U(., .)$ is the uniform distribution.

The differences between the true IF and the model of increments of the blood, \mathbf{g} , are assumed to have an unknown variance ψ . The prior distributions for the parameters of the IF and the tissue images are

$$f(\mathbf{g} | \psi) = N(\mathbf{0}_{n \times 1}, \psi^{-1} I_n), \quad f(\psi) = G(\zeta_0, \eta_0), \quad (8)$$

$$f(\mathbf{a}_f | v_f) = tN(\mathbf{0}_{p \times 1}, v_f^{-1} I_p), \quad f(v_f) = G(\alpha_{f,0}, \beta_{f,0}), \quad (9)$$

where v_f is a hyperparameter that allows to select the number of relevant tissue images, r , via the automatic relevance determination (ARD) approach (Bishop and Tipping 2000). The ARD approach is based on the assumption that the expected value of the variance of a redundant parameter approaches zero in the VB solution.

In further text, this model will be denoted as the blind compartment model separation (BCMS).

2.2.1 Alternative model of the IF

The incremental model of IF (3) is one of many possible parameterisations. For comparison, we also consider direct estimation of the IF \mathbf{b} . Since we are using probabilistic approach, we also need to specify model of variance of all elements of \mathbf{b} . Assuming unknown mutually independent variance of each element b_i of the IF, we model

$$f(b_i | \psi_i) = N(0, \psi_i^{-1}), \quad (10)$$

$$f(\psi_i) = G(\zeta_{i,0}, \eta_{i,0}), \quad (11)$$

where ψ_i is the unknown precision (inverse variance) of element b_i , and (11) is its conjugate prior (Tipping and Bishop 1999). Model (10) and (11) is commonly known as ARD (Tipping and Bishop 1999).

2.3 VB solution

VB method (Miskin 2000; Šmídl and Quinn 2006) is a technique for assessment of shaping parameters θ of

posterior distribution $f(\theta|D)$. A parametric probabilistic model of the observation is given as $f(D|\theta)$, data D are conditioned by multivariate parameter $\theta = [\theta_1, \dots, \theta_q]'$. The task is to find out a distribution $\check{f}(\theta|D)$ which should be as close as possible to the true posterior distribution $f(\theta|D)$. Formally,

$$\check{f}(\theta|D) = \arg \min_{\check{f} \in \mathbf{F}_c} \Delta(\check{f}(\theta|D) || f(\theta|D)), \quad (12)$$

where $\Delta(f||g)$ is a measure between functions f and g and \mathbf{F}_c is the space of conditionally independent functions. The VB method selects as the measure the Kullback–Leibler divergence (KLD) (Kullback and Leibler 1951), i.e. $\Delta \equiv \text{KLD}$, which is defined as

$$\text{KLD}(\check{f}(\theta|D) || f(\theta|D)) = \int \check{f}(\theta|D) \ln \frac{\check{f}(\theta|D)}{f(\theta|D)} d\theta. \quad (13)$$

Then, the shaping parameters of posterior distribution can be found using the VB theorem.

Let $f(\theta|D)$ be the posterior distribution of multivariate parameter $\theta = [\theta_1, \dots, \theta_q]'$. Let $\check{f}(\theta|D)$ be an approximate distribution restricted to the set of conditionally independent distributions as

$$\check{f}(\theta|D) = \prod_{i=1}^q \check{f}(\theta_i|D). \quad (14)$$

Then, the minimum of KLD, i.e.

$$\check{f}(\theta|D) = \arg \min_{\check{f} \in \mathbf{F}_c} \text{KLD}(\check{f}(\theta|D) || f(\theta|D)), \quad (15)$$

is reached for

$$\check{f}(\theta_i|D) \propto \exp\left(E_{\check{f}(\theta_i|D)}[\ln(f(\theta, D))]\right), \quad i = 1, \dots, q, \quad (16)$$

where symbol \propto means up to normalising constant, $E_f(\cdot)$ means expected value of an argument with respect to distribution f and $\theta_{/i}$ denotes complement of θ_i in θ ; hence, $\theta_{/i} = [\theta_1, \dots, \theta_{i-1}, \theta_{i+1}, \dots, \theta_q]$.

Proof can be found in Miskin (2000).

We will formulate the steps of the VB method in the sense of Šmídl and Quinn (2006). The first step is a formulation of the observation model $f(D|\theta)$ and prior distributions of parameters $f_i(\theta_i)$ followed by construction of the joint distribution of parameters and observed data $f(\theta, D)$. The fundamental assumption necessary for analytical tractability of the method is that joint distribution is from separable-in-parameters family (Šmídl and Quinn 2006):

$$\ln f(\theta_1, \theta_2, D) = f_1(\theta_1, D) f_2(\theta_2, D) \quad (17)$$

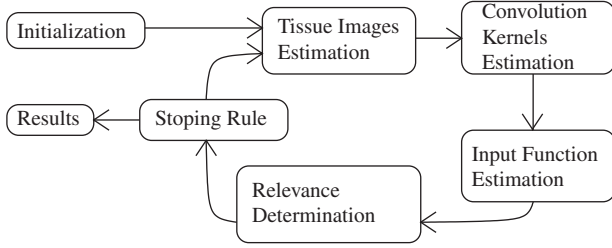


Figure 1. The computation scheme of the BCMS algorithm.

is an example for two parameters model. The next step is computing the VB marginals using the VB theorem (16).

In the following step, the standard parametric posterior distributions are identified from $\tilde{f}(\theta_i|D)$ as

$$\tilde{f}(\theta_i|D) \equiv f_i(\theta_i|\psi_i), \quad \forall i, \quad (18)$$

where ψ_i is vector with parameters of selected standard distribution. The equations for parameters ψ_i can be established where the expectations of parameters of other distributions are taken as temporary constants. This step forms a set of implicit equations together with formulations of moments of standard distributions used in (18). The set can be solved iteratively with selected prior parameters and starting points of estimates. The selection should be done carefully since only convergence to a local minimum is guaranteed.

Following the VB method, the optimal approximative posterior densities (18) were identified to be

$$\tilde{f}(\mathbf{g}|D, r) = N(\mu_{\mathbf{g}}, \Sigma_{\mathbf{g}}), \quad \tilde{f}(\psi|D, r) = G(\zeta, \eta), \quad (19)$$

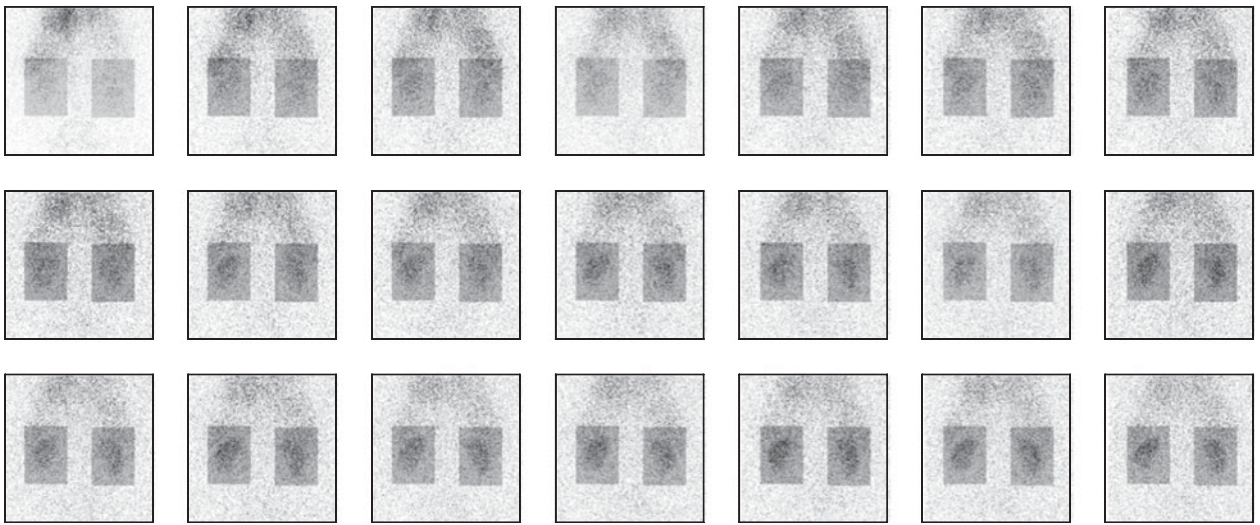


Figure 2. The uptake part of the scintigraphic sequence. Rough rectangular ROIs placed on left and right kidneys are visualized by darker colour.

$$\tilde{f}(\text{vect}(W)|D, r) = tN(\mu_{\text{vect}(W)}, \Sigma_{\text{vect}(W)}), \quad (20)$$

$$\tilde{f}(\xi_f|D, r) = G(\kappa_f, \nu_f),$$

$$\tilde{f}(A|D, r) = tN(\mu_A, I_p \otimes \Phi_A), \quad (21)$$

$$\tilde{f}(v_f|D, r) = G(\alpha_f, \beta_f),$$

$$\tilde{f}(\omega|D, r) = G_\omega(\vartheta, \rho). \quad (22)$$

Note that vectorised form of matrix $W = [\mathbf{w}_1, \dots, \mathbf{w}_r]$, $\text{vect}(W)$, has to be used for computation reason. Shaping parameters

$$\mu_{\mathbf{g}}, \Sigma_{\mathbf{g}}, \zeta, \eta, \mu_{\text{vect}(W)}, \Sigma_{\text{vect}(W)}, \kappa_f, \nu_f, \mu_A, \Phi_A, \alpha_f, \beta_f, \vartheta, \rho$$

of posterior distributions (19)–(22) are forming the set of implicit equations given in Appendix A. The equations need to be solved iteratively. The computation scheme is shown in Figure 1. Each experiment runs till the hyperparameters ν_f are stabilised.

VB solution for Model (10) and (11) is a straightforward modification of Equations (A2), (A8) and (A9) from the BCMS model.

3. Experiments and results

The iterative algorithm was tested on the dataset from planar renal scintigraphy. In this modality, the pixels of the images are obtained as counts of radioactive particles observed by a scintillation camera. The principle of the imaging is described in Di Paola et al. (1982) and its key properties are relatively low resolution and Poisson-distributed noise. Therefore, the observed images are scaled using correspondence analysis (Benali et al. 1993)

to match the assumptions of homogeneous noise (4). Since the camera registers radioactive particles from all depths of the body, the image is a 2D projection of the whole body. Therefore, each pixel contains contributions from organs from different depths of the body which is modelled by superposition of r organs in (1).

A typical sequence contains 180 images of 128×128 pixels recorded in 10 s interval. For detailed analysis, we typically select only some pixels (via the rough rectangular ROI) and either all images or the initial part of the sequence known as the uptake (Durand et al. 2008). Detection of the uptake time is manual and the same part is used for all compared methods.

The BCMS algorithm provides results in the form of tissue images, a_f , tissue-specific convolution kernel, u_f and IF, b . Results of the application of the BCMS algorithm to the ROI of the right kidney of the uptake part of the scintigraphic sequence shown in Figure 2 are displayed in Figure 3. For these data, the ARD property of the algorithm selected two structures to be relevant which corresponds well with biological assumptions. The estimates corresponding to the background are displayed in the first row, those corresponding to the parenchyma in the second row.

In the following sections, we apply the BCMS algorithm to available datasets from clinical renal scintigraphy. First, we test the performance of the algorithm for estimation of the DRF and provide statistical comparison to competing methods. Second, we use the database that contains 19 patients with estimated TACs of parenchyma by an experienced physician. Third, we study estimates properties of the estimated IFs on both datasets.

3.1 DRF estimation

DRF (Gordon et al. 2011) is mathematically simple but clinically important and a hardly obtainable parameter. It is defined as

$$\text{DRF}_L = \frac{L_p}{L_p + R_p}, \quad (23)$$

where DRF_L is DRF for the left kidney, L_p is the total activity of the left parenchyma (i.e. one of the tissues from decomposition (1)) and R_p is the total activity in the right parenchyma. The parenchyma is the spongy tissue covering the whole kidney which accumulates the activity from the blood. The DRF is traditionally computed on the uptake part of the sequence, i.e. the interval when the kidney only accumulates the activity without secretion and only the parenchyma-part of the kidney is activated (Durand et al. 2008).

In this section, four methods are applied to the dataset and their results are compared: two manual and three

semi-automatic.

- (i) Reference manual method (**RMM**): The assessment of DRF is typically based on manual drawing of the ROIs of parenchyma; however, details of subsequent evaluation differ from one hospital to another (Caglar et al. 2008; Brink et al. 2012). The studied dataset already provides results of the DRF analysis obtained by an experienced physician using a range of methods including the Patlak–Rutland plot (Patlak et al. 1983), crosschecking with the deconvolution method (Kuruc et al. 1982).
- (ii) Common BSS (**BSS +**) method: The task of decomposition of the observed data into a superposition of a product of two unknowns (Equation (1)) has been studied in the BSS literature. Specifically, the method described in (Miskin 2000) is based on the same assumptions as the proposed BCMS method, except for the convolution model. Comparison with this method then allows to study the influence of this modelling choice to the results.
- (iii) Factor analysis with integrated regions of interest (**FAROI**s): The BSS problem has several extensions such as (Šmídl and Tichý 2012). Here, the TACs are modelled in the same way as in the BSS + method; however, the tissue images are assumed to be sparse. The sparsity is imposed using mixture modelling where switching between mixtures is done using probabilistic parameter $\mathbf{i} \in [0, 1]$ for each pixel. This forms an automated probabilistic ROI for each tissue image.
- (iv) Straightforward manual method (**SMM**): This an example of another commonly used approach. Four ROIs are manually drawn for each dataset in our case by a trained novice. These are the left and the right kidneys, and the left and the right backgrounds on the outer side of the kidneys. The activity of the reference backgrounds is subtracted from the activity in the related kidneys. It is assumed that the same background is behind (or in front of) the kidney.
- (v) Semi-automatic BCMS-based method (**BCMS**): The operator is asked to place two rectangular ROIs around each kidney. The BCMS method is applied to each of these rectangular ROIs to obtain estimates of two underlying structures (as demonstrated in Figure 3). The estimate of the parenchyma images is thresholded at $0.5 \times$ maximum of the image to remove remaining traces of the background.
- (vi) Semi-automatic BCMS-based method with an alternative model of the IF (10 and 11) (**BCMSard**). Otherwise identical to the BCMS method.

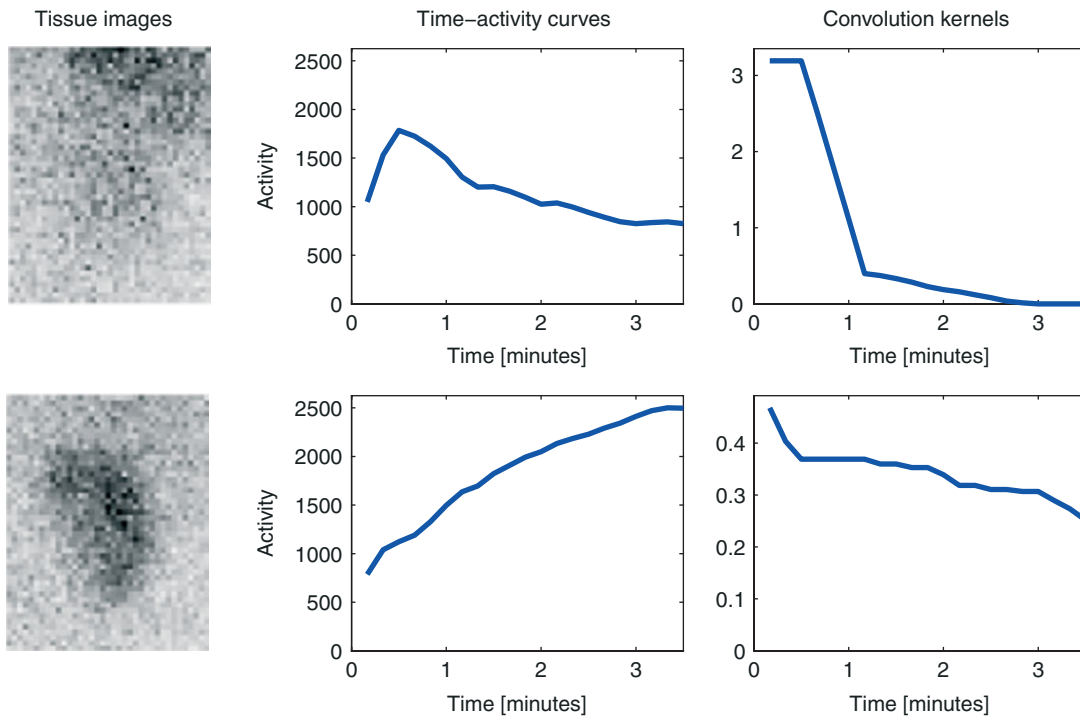


Figure 3. Estimates provided by the BCMS algorithm for a selected dataset, right ROI. Left: estimated tissue images; middle: estimated TAC; right: estimated tissue-specific kernel.

3.1.1 Statistical comparison

The four described methods will be compared via difference of their results of DRF from those provided by the experienced expert (RMM) as a reference value. Since the expert considered all assumptions of the approach in his evaluation, we will consider the automatic method that is closer to his results to be better. The DRF estimates from the expert are publicly available in VFN Praha (2013) for 99 patients with both kidneys as well as source data and their detailed description. We applied all introduced methods to this dataset and display the results of the estimated DRF for each method in Table 1 via quantiles of their differences from the reference value. Note that the estimates of the BCMS method are systematically closer to the reference values than those of the competing methods. The computation time of the semi-automatic methods (ii), (iii) and (v) is comparable,

Table 1. Quantiles of the difference of the estimated DRFs from the reference value for all 99 patients.

Method	<5%	<10%	10%
BSS +	39.6%	82.2%	18.8%
FAROI	54.5%	84.8%	15.2%
SMM	36.5%	70.8%	29.2%
BCMS	63.5%	89.6%	10.4%
BCMSard	66.7%	87.9%	12.1%

Note: Bold value denotes the best result.

one sequence is processed under 1 min. The maximum number of tissues is set to $r = 3$.

The results for the patients with diagnosed abnormality in kidney function are shown in Table 2. There is significantly lower signal, hence, the spread of the errors is much higher. Note that manual analysis of these data is much more demanding, since the trained novice (line SMM in Table 2) achieved the worst results. However, this variance in results is suppressed when the analysis is performed by experienced experts as shown in Brink et al. (2012), where maximum–minimum difference was less than 6% in large majority of the cases. The worst reproducibility was observed for data from children with low glomerular filtration rate.

From the compared methods, the BCMS method is the closest to the reference results, on both the full dataset (Table 1) and the selected abnormal cases (Table 2).

Table 2. Quantiles of the difference of the estimated DRF from the reference value for the patients with diagnosed abnormality in kidney function.

Method	<5%	<10%	10%
BSS +	39.1%	69.6%	30.4%
FAROI	45.3%	75.5%	24.5%
SMM	17.4%	47.8%	52.2%
BCMS	58.7%	80.4%	19.6%
BCMSard	64.2%	79.2%	20.8%

Note: Bold value denotes the best result.

Table 3. Statistical evaluation of differences between the estimated TACs from the reference TAC from the physician.

Algorithm	$\mu_{\text{MSE}} \pm \sigma_{\text{MSE}}$	$\mu_{\text{MAE}} \pm \sigma_{\text{MAE}}$	Best MSE	Best MAE
BSS +	0.0314 ± 0.0340	0.1197 ± 0.0687	7	8
FAROI	0.0358 ± 0.0469	0.1202 ± 0.0860	13	11
BCMS	0.0207 ± 0.0296	0.0914 ± 0.0601	18	19
BCMSard	0.0270 ± 0.0323	0.1060 ± 0.0690	N/A (7)	N/A (8)

Notes: The competing methods are compared in terms of the average mean and absolute error over all 38 TACs. The number of TACs for which a particular method provided the best MSE and MAE is also displayed.

3.2 Experiment with expert TACs reference

We have studied clinical data from 19 patients, i.e. 38 image sequences for kidneys. In this dataset, an experienced physician selected the parenchyma structures, subtracted vascular backgrounds and other tissues from these, and provided the TACs of the parenchyma tissues. These values will be used as references for comparison of the proposed methods and its competitors. The BSS+, FAROI, BCMS and BCMSard algorithms are applied to rough rectangular ROI of each kidney, and the tissue related to the parenchyma structure is automatically detected. The expected number of tissues is set to $r = 4$. The SMM was not used due to poor performance in the previous experiment. Since we do not have a direct comparable scale of the TACs, all TACs of the parenchyma (or its estimate) are scaled to have minima at 0 and maxima at 1. Estimates of the parenchyma for a selected kidney are given in Figure 4 for illustration. To perform a quantitative evaluation, we compute the mean square error (MSE) and the mean absolute error (MAE) for each TAC,

$$\text{MSE}_i = \frac{1}{n} \sum_{j=1}^n \left(x_{j,\text{par}}^{(i)} - x_{j,\text{par}}^{\text{ref},(i)} \right)^2, \quad (24)$$

$$\text{MAE}_i = \frac{1}{n} \sum_{j=1}^n \left| x_{j,\text{par}}^{(i)} - x_{j,\text{par}}^{\text{ref},(i)} \right|,$$

where $\mathbf{x}_{\text{par}}^{(i)}$ is the TAC of parenchyma from the i th studied sequence and $\mathbf{x}_{\text{par}}^{\text{ref},(i)}$ is the reference TAC of the same sequence from the physician.

The methods are compared in terms of average MSE and MAE over all 38 TACs,

$$\mu_{\text{MSE}} = \frac{1}{38} \sum_{i=1}^{38} (\text{MSE}_i), \quad (25)$$

$$\sigma_{\text{MSE}} = \sqrt{\frac{1}{38-1} \sum_{i=1}^{38} (\text{MSE}_i - \mu_{\text{MSE}})^2},$$

and analogically for MAE.

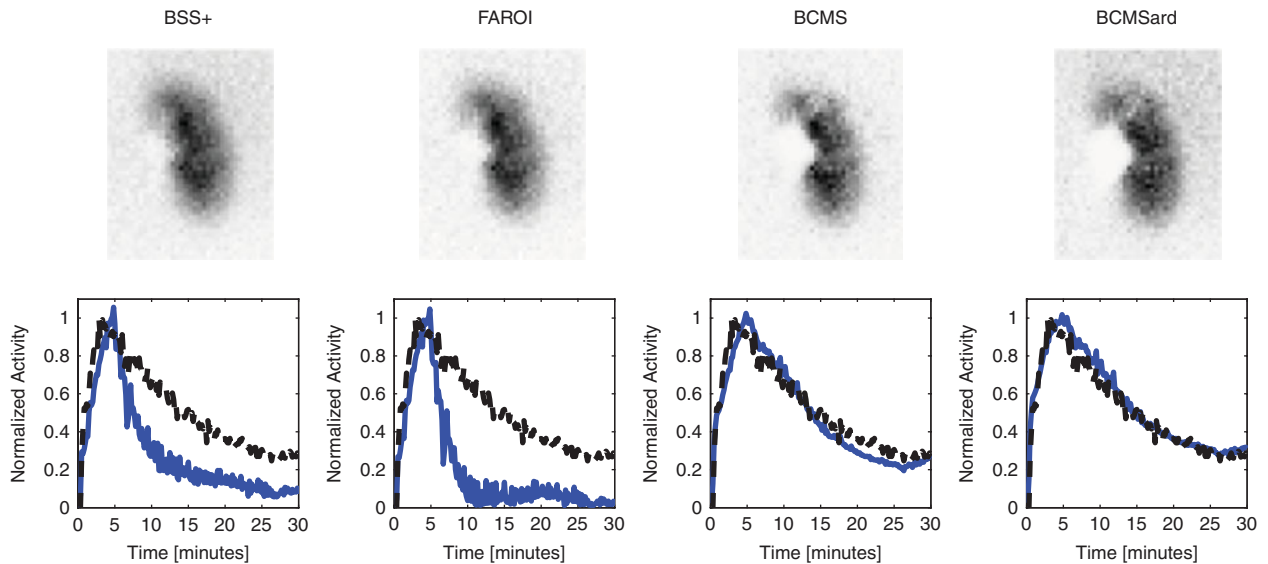


Figure 4. Estimates of the parenchyma tissue images (upper row) and associated TACs (bottom row) for four tested automated methods: BSS + (left column), FAROI (middle left column), the proposed BCMS algorithms (middle right column) and the BCMSard (right column). The estimates of the TACs (full line) are compared with the reference from the expert physician (dashed line).

The results are displayed in Table 3. The BCMS algorithm outperforms all other algorithms in terms of average MSE and MAE. We note that each tested method was able to provide the best estimated for some tested kidneys. However, the BCMS provided the best result in more cases than other methods. The main advantage of the BCMS is, however, its consistency throughout the tested dataset. This is demonstrated by the boxplot visualization of the full distribution of MSE errors for the tested dataset (Figure 5).

3.3 IFs estimation

The estimate of the IF is an output of the BCMS algorithm. Since the ground truth of the IF is not available, we propose the following experimental validation. First, we compute IFs for both left and right ROIs of kidneys

separately. Second, we compare estimates of the IF for the left and the right kidneys. If the model assumption (2) is valid, the estimates should be very close to each other.

The BCMS algorithm was run on non-overlapping ROIs of the left and right kidneys for both datasets used above. Histogram of the differences in the estimated IFs for all 118 patients is displayed in Figure 6 via histogram of differences

$$\Delta_i = \sum_{j=1}^n \left| \bar{b}_j^{(\text{left})} - \bar{b}_j^{(\text{right})} \right|, \quad (26)$$

where $\bar{b}_j^{(\text{left})}$ denotes estimate of the IF from the ROI of the left kidney scaled to unit area $\bar{b}_j = b_j / \sum_{j=1}^n b_j$. In effect, difference (26) denotes the area of the differences (AODs) between these curves. The estimated IFs for two selected sequences are displayed in Figure 7. These were

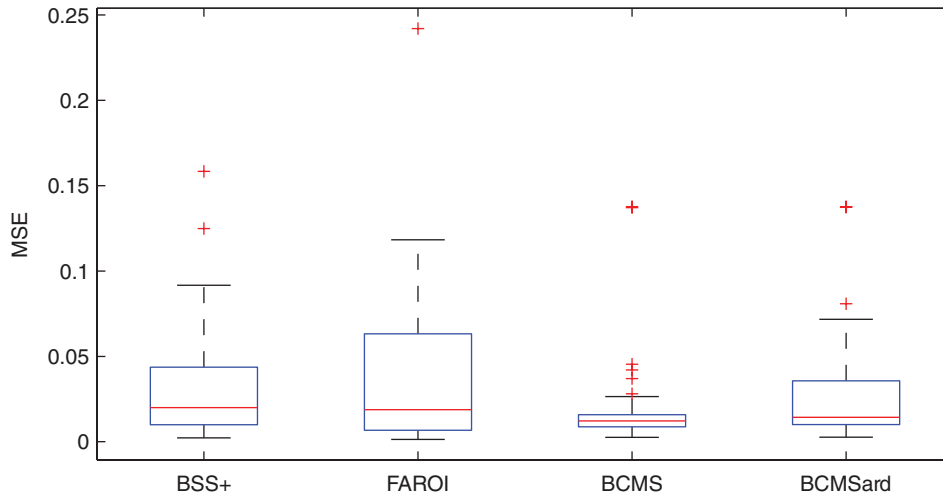


Figure 5. Boxplots of distribution of the MSE for all 38 datasets.

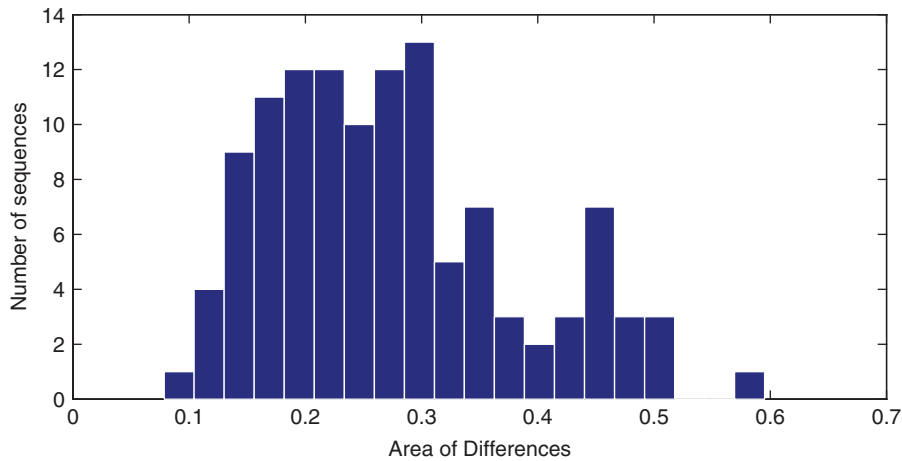


Figure 6. Histogram of difference between IFs obtained for the left and the right ROIs.

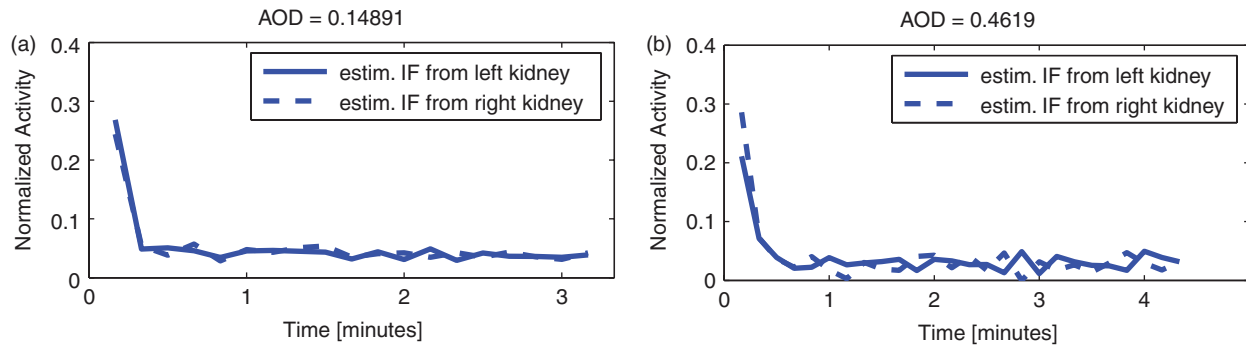


Figure 7. Estimated IFs for two selected sequences. AODs between IFs from the left and the right ROIs is 0.1489 (left) and 0.4619 (right).

selected from both sides of the histogram in Figure 6, with AODs 0.1489 and 0.4619, respectively. We conjecture that even in the case of the worse result, Figure 7 (right), the IFs well correspond to each other and the difference can be contributed to the noise. Note that the AOD is less than 0.3 for the majority of the tested sequences. Differences for the BCMSard are completely analogical.

4. Discussion and future work

The work presented in this paper is one of the first steps towards fully automatic kinetic analysis of dynamic medical sequences. The modelling choices made in this paper are based on models from the literature; however, with more available data, more accurate and demanding models can be tested. Examples of such extensions are now discussed.

The presented semi-automatic method of DRF analysis was run with manual intervention in two key steps: (i) positioning of the rectangular ROIs to contain the left and right kidneys and (ii) selection of the uptake part of the sequence. While the first step is relatively easy to automate and seldom requires intervention, the second step is more demanding. Specifically, we select the uptake part to start at the peak of the vascular activity in the ROI of the kidney. The end of the sequence is determined by the peak of the parenchyma activity. More detailed modelling of the sequence is needed to achieve the fully automated method.

Note that the BCMS algorithm assumes that each tissue is activated in the beginning of the sequence. The assumption is valid for the given experiments; however, the assumption is not met, e.g. for pelvis tissue within the kidney of the urinary bladder. The BCMS algorithm is valid well for parenchyma tissue but more detailed modelling is necessary for general validity of the model.

The proposed BCMS method is able to provide both the IF and the organ function. The results presented in

Section 3 suggest that the estimated IF is reliable, and estimates of IFs from the left and right kidneys are comparable. Some disproportion can be explained by the background tissue, it is also possible that the estimate is only a local minimum in the space of possible solutions. Also, the model assumption may not be appropriate for the given patient. A dataset that would also have the IF measured by blood sampling would be necessary to resolve this issue.

Sensitivity of the method to the chosen model of the IF is demonstrated by different performances of the BCMS and BCMSard methods. The essential difference of these two models is different model of variance of the IF. The BCMS model was found to be superior in the experimental evaluation. We conjecture that this is due to the presence of correlation between the elements of \mathbf{b} due to incremental parametrisation.

5. Conclusion

A probabilistic model of medical image sequences and its Variational Bayesian solution for functional analysis of medical data were proposed. TACs are modelled as convolution of an unknown IF with kernels. The shape of each kernel is restricted to a piecewise-linear curve to match the fluid behaviour in kidneys. The resulting algorithm thus achieves blind separation of compartment models with a common IF. No manual intervention is required in this process. We have shown that the estimated IF and organ function correspond well with the biological expectations. Since the method does not use any modality-specific assumptions, it can be used in any other modality.

The algorithm was further applied to semi-automatic analysis of DRF from scintigraphic data. Manual intervention was required to select the uptake part of the sequence and the position of the rectangular areas containing the left and the right kidneys. The results were compared with those of two completely manual methods and a common BSS method with the same level of intervention. The most

sophisticated manual method performed by an experienced expert was selected as a reference value. On a dataset of 99 patients, the estimates of DRF provided by the proposed BCMS method were found to be systematically closer to the reference value than those of any other method. Furthermore, the experiment with 19 patients was given where an experienced physician manually obtained TACs of parenchyma. We have shown that the BCMS algorithm outperforms other algorithms in the sense of MSE or MAE between automatic estimates and those obtained manually by the physician.

The MATLAB implementation of the BCMS algorithm is available for download from http://www.utia.cas.cz/AS/softwaretools/image_sequences

Funding

This work was supported by the Czech Science Foundation [grant number 13-29225S].

Notes

1. Email: smidl@utia.cas.cz
2. Email: samal@cesnet.cz

References

- Benali H, Buvat I, Frouin F, Bazin J, Paola R. 1993. A statistical model for the determination of the optimal metric in factor analysis of medical image sequences (FAMIS). *Phys Med Biol.* 38:1065.
- Bishop C, Tipping M. 2000. Variational relevance vector machines. In: *Proceedings of the 16th Conference on Uncertainty in Artificial Intelligence*. San Francisco (CA): Morgan Kaufmann p. 46–53.
- Brink A, Šámal M, Mann M. 2012. The reproducibility of measurements of differential renal function in paediatric 99mTc-MAG renography. *Nucl Med Commun.* 33(8):824–831.
- Caglar M, Gedik G, Karabulut E. 2008. Differential renal function estimation by dynamic renal scintigraphy: influence of background definition and radiopharmaceutical. *Nucl Med Commun.* 29(11):1002–1005.
- Chen L, Choyke P, Chan TH, Chi CY, Wang G, Wang Y. 2011. Tissue-specific compartmental analysis for dynamic contrast-enhanced MR imaging of complex tumors. *IEEE Trans Med Imaging.* 30(12):2044–2058.
- Dempster AP, Laird NM, Rubin DB. 1977. Maximum likelihood from incomplete data via the EM algorithm. *J Royal Stat Soc.* 39(1):1–38.
- Di Paola R, Bazin JP, Aubry F, Aurengo A, Cavailloles F, Herry JY, Kahn E. 1982. Handling of dynamic sequences in nuclear medicine. *IEEE Trans Nucl Sci.* 29(4):1310–1321.
- Durand E, Blaufox MD, Britton KE, Carlsen O, Cosgriff P, Fine E, Fleming J, Nimmon C, Piepsz A, Prigent A, et al. 2008. International Scientific Committee of Radionuclides in Nephrourology (ISCORN) consensus on renal transit time measurements. *Semin Nucl Med.* 38:82–102.
- Garcia E, Folks R, Pak S, Taylor A. 2010. Totally automatic definition of renal regions-of-interest from 99mTc-MAG3 renograms: validation in patients with normal kidneys and in patients with suspected renal obstruction. *Nucl Med Commun.* 31(5):366–374.
- Germano G, Chen BC, Huang S-C, Gambhir SS, Hoffman EJ, Phelps ME. 1992. Use of the abdominal aorta for arterial input function determination in hepatic and renal pet studies. *J Nucl Med.* 33(4):613.
- Ghahramani Z, Beal M. 2001. Graphical models and variational methods. In: *Opper M, Saad D, editors. Advanced mean field methods*. Cambridge (MA): MIT Press. p. 161–177.
- Gordon I, Piepsz A, Sixt R. 2011. Guidelines for standard and diuretic renogram in children. *Eur J Nucl Med Mol Imaging.* 38(6):1175–1188.
- Greuter HNJM, Boellaard R, van Lingen A, Franssen EJJ, Lammertsma AA. 2003. Measurement of 18F-FDG concentrations in blood samples: comparison of direct calibration and standard solution methods. *J Nucl Med Technol.* 31(4):206–209.
- Kullback S, Leibler R. 1951. On information and sufficiency. *Ann Math Stat.* 22(1):79–86.
- Kuruc A, Caldicott W, Treves S. 1982. Improved deconvolution technique for the calculation of renal retention functions. *Comput Biomed Res.* 15(1):46–56.
- Margadán-Méndez M, Juslin A, Nesterov S, Kalliokoski K, Knuuti J, Ruotsalainen U. 2010. ICA based automatic segmentation of dynamic H215 O cardiac PET images. *IEEE Trans Inform Technol Biomed.* 14(3):795–802.
- Miskin J. 2000. Ensemble learning for independent component analysis [dissertation]. Cambridge, UK: University of Cambridge.
- Patlak CS, Blasberg RG, Fenstermacher JD. 1983. Graphical evaluation of blood-to-brain transfer constants from multiple-time uptake data. *J Cereb Blood Flow Metab.* 3(1):1–7.
- Riabkov D, Di Bella E. 2002. Estimation of kinetic parameters without input functions: analysis of three methods for multichannel blind identification. *IEEE Trans Biomed Eng.* 49(11):1318–1327.
- Šmídl V, Quinn A. 2006. *The Variational Bayes method in signal processing*. Heidelberg: Springer.
- Šmídl V, Tichý O. 2012. Automatic regions of interest in factor analysis for dynamic medical imaging. In: *2012 IEEE International Symposium on Biomedical Imaging (ISBI)*. Barcelona: IEEE. p. 158–161.
- Tipping M, Bishop C. 1999. Probabilistic principal component analysis. *J Royal Stat Soc Ser B (Stat Method).* 61(3): 611–622.
- VFN Praha. 2013. Database of dynamic renal scintigraphy. Available from: www.dynamicrenalstudy.org
- Vriens D, de Geus-Oei L, Oyen W, Visser E. 2009. A curve-fitting approach to estimate the arterial plasma input function for the assessment of glucose metabolic rate and response to treatment. *J Nucl Med.* 50(12):1933–1939.

Appendix A. Shaping parameters of posterior distributions

The shaping parameters of posterior distributions (19)–(22) are given as follows:

$$\Phi_A = (\hat{\omega}\hat{X}'\hat{X} + \hat{Y})^{-1}, \quad \mu_A = (\hat{\omega}\hat{D}\hat{X})\Phi_A, \quad (\text{A1})$$

$$\Sigma_g = \left(\hat{\psi}\hat{I}_n + \hat{\omega}C' \sum_{i,j=1}^r \left(\hat{\mathbf{a}}'_i \hat{\mathbf{a}}_j \sum_{k,l=1}^n \Delta'_k \Delta_l \mu_{k+1,j} \mu_{l+1,i} \right) C \right)^{-1},$$

$$\mu_g = \hat{\omega} \Sigma_g C' \sum_{i=1}^r \left(\left(\sum_{k=0}^{n-1} \Delta'_k \mu_{k+1,i} \right) D' \hat{a}_i \right), \quad (\text{A2})$$

$$\Sigma_{\text{vect}(W)} = \left(\left((\hat{A}'\hat{A}) \otimes \hat{\omega}C' \hat{B}' \hat{B} C \right) + \left(\hat{\Xi}_W \otimes I_n \right) \right)^{-1}, \quad (\text{A3})$$

$$\mu_{\text{vect}(W)} = \Sigma_{\text{vect}(W)} \left(\hat{\Xi}_W \text{vect} \left(\left(C' \hat{B}' \hat{B} C \right)^{-1} C' \hat{B} D' \hat{A} (\hat{A}'\hat{A})^{-1} \right) + \left(\hat{\Xi}_W \otimes I_n \right) \text{vect}(\hat{M}_W) \right), \quad (\text{A4})$$

$$\nu = \nu_0 + \frac{1}{2} \text{diag}(\hat{W}'\hat{W}) + \frac{1}{2} \text{diag}(-2\hat{W}'\hat{M}_W) + \frac{1}{2} \text{diag}(M'_W \hat{M}_W), \quad (\text{A5})$$

$$\rho = \rho_0 + \frac{1}{2} \text{tr}(DD' - 2\hat{A}\hat{X}'D') + \frac{1}{2} \text{tr}(A\hat{X}'\hat{X}A'), \quad (\text{A6})$$

$$\alpha = \alpha_0 + \frac{p}{2} \mathbf{1}_{r,1}, \quad \beta = \beta_0 + \frac{1}{2} \text{diag}(\hat{A}'\hat{A}), \quad (\text{A7})$$

$$\kappa = \kappa_0 + \frac{n}{2} \mathbf{1}_{r,1}, \quad \zeta = \zeta_0 + \frac{n}{2}, \quad (\text{A8})$$

$$\eta = \eta_0 + \frac{1}{2} \text{tr}(\hat{\mathbf{g}}'\hat{\mathbf{g}}), \quad \vartheta = \vartheta_0 + \frac{np}{2}, \quad (\text{A9})$$

where \hat{x} denotes estimate of variable x , X is the matrix with TACs in its columns, \otimes denotes the Kronecker product, M_W contains prior vectors of W composed of estimates of h , s and l (obtained using EM algorithm (Dempster et al. 1977)), auxiliary matrix $\Delta_k \in \mathbf{R}^{n \times n}$ is defined as

$$(\Delta_k)_{ij} = \begin{cases} 1, & \text{if } i - j = k, \\ 0, & \text{otherwise,} \end{cases}$$

auxiliary matrices $C \in \mathbf{R}^{n \times n}$ and $B \in \mathbf{R}^{n \times n}$ are defined as

$$C = \begin{pmatrix} 1 & 1 & \cdots & 1 & 1 \\ 0 & 1 & \cdots & 1 & 1 \\ \vdots & \vdots & \ddots & \vdots & \vdots \\ 0 & 0 & \cdots & 0 & 1 \end{pmatrix}, \quad B = \begin{pmatrix} b_1 & 0 & \cdots & 0 \\ b_2 & b_1 & \cdots & 0 \\ \vdots & \vdots & \ddots & \vdots \\ b_n & b_{n-1} & \cdots & b_1 \end{pmatrix}, \quad (\text{A10})$$

where b_1, \dots, b_n are elements from vector of IF \mathbf{b} , and $\mathbf{1}_{r,1}$ is a matrix of those of the given size.

The required moments are computed according to, e.g. appendix in Šmíd and Quinn (2006).